SIMULATION OF HOLLOW ELECTRON BEAM COLLIMATION IN THE FERMILAB TEVATRON COLLIDER*

I. Morozov, G. Stancari, A. Valishev, Fermilab, Batavia, IL 60510, USA
D. Shatilov, BINP SB RAS, Novosibirsk, Russia

Abstract

The concept of augmenting the conventional collimation system of high-energy storage rings with a hollow electron beam was successfully demonstrated in experiments at the Tevatron. A reliable numerical model is required for understanding particle dynamics in the presence of a hollow beam collimator. Several models were developed to describe imperfections of the electron beam profile and alignment. The features of the imperfections are estimated from electron beam profile measurements. Numerical simulations of halo removal rates are compared with experimental data taken at the Tevatron.

INTRODUCTION

The collimation system is vital for the operation of high-power accelerators. The classic multi-stage collimation system is robust and efficient, but it has limitations, such as leakage, impedance, loss spikes during setup, and losses due to beam jitter. One possible option to address these limitations is to include a hollow electron beam collimator (HEBC) [1, 2]. The HEBC is a cylindrical, hollow, magnetically confined, possibly pulsed electron beam overlapping with the beam halo. Electrons enclose the circulating beam. Halo particles are kicked transversely by the electromagnetic field of the electrons. If the hollow charge distribution is axially symmetric, the core of the circulating beam does not experience any electric or magnetic fields. The transverse kicks are small and tunable, so that the device acts more like a 'soft scraper,' rather than a hard aperture limitation. If needed, the electron beam can be pulsed resonantly with betatron oscillations to remove particles faster.

The concept of hollow electron beam collimation was tested experimentally in the Fermilab Tevatron collider [3]. The electron current density profile was measured on a separate test stand by recording the current through a pinhole in the collector while changing the position of the beam in small steps (Fig. 1). This profile is close to the profile used in experiments at the Tevatron.

A reliable numerical model is required for complete understanding of particle dynamics in the presence of a hollow beam collimator. Here we develop several numerical models of the HEBC. Model parameters are taken from electron profile measurements. The main results of simulations and a comparison with experimental data are given.
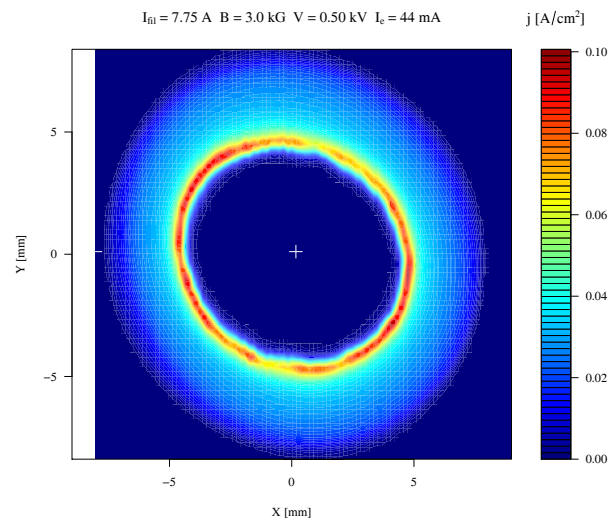
Figure 1: Example of measured hollow electron beam transverse profile.

NUMERICAL MODELS

Because the effects of the HEBC were measured over several hours, numerical simulations require a globally accurate integration scheme. We have chosen a drift-kick scheme to include the symplectic condition and to keep our model simple. To obtain an analytical expression for kicks, the electron beam is assumed to be infinite in the longitudinal direction. Only transverse field components are then present. Kicks can be expressed as a function of the electron beam rest frame electric field $\vec{E}_\perp$ as follows:

$$\Delta \vec{p}_\perp = \Delta s \frac{q}{\beta_b c p_b} \gamma_e (1 \pm \beta_e \beta_b) \vec{E}_\perp, \qquad (1)$$

where $\beta_b c$ and p_b are the circulating particle velocity and momentum, β_e and γ_e are the relativistic electron beam parameters, and the plus sign corresponds to $\vec{\beta}_e \cdot \vec{\beta}_p < 0$ (in which case the transverse kick is maximum). Both an ideal HEBC model and several models with transverse imperfections (angular harmonics, distortion of the radial density profile) can be developed based on the particular form of the electric field.

Electron beam alignment was implemented using the local Euclidean group [4]. Simulations of translations and rotations have shown no significant effect for typical alignment errors. Only a general discussion is presented on the effects of bends in the electron beam (edge effects).
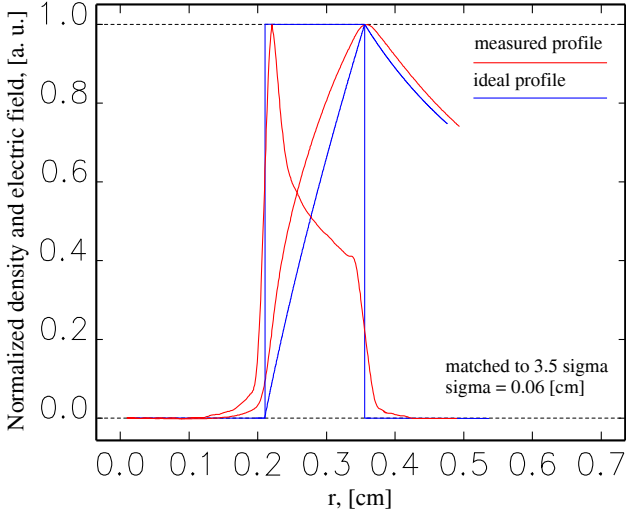
Figure 2: Normalized electron beam radial density profile and electric field for a flat ('ideal') HEBC (blue) and for an HEBC with nonuniform radial profile (red).

Figure 3: Angular distribution function (top) and corresponding relative harmonic amplitudes (bottom).

For the ideal HEBC model, the charge density is constant between the inner radius r_1 and the outer radius r_2 (Fig. 2, blue curve). Substitution of the radial electric field into Eq. 1 yields the following radial kicks:

$$\Delta p_r = \begin{cases} 0 & r < r_1 \\ 2\Omega_e \dfrac{r^2 - r_1^2}{r(r_2^2 - r_1^2)}\Delta s & r_1 < r < r_2 \\ 2\Omega_e \dfrac{1}{r}\Delta s & r_2 < r, \end{cases} \qquad (2)$$

where Ω_e is defined as

$$\Omega_e = 0.3 \times 10^{-7} \frac{I_e[\text{A}]}{p_b[\text{GeV/c}]} \gamma_e \frac{1 + \beta_e \beta_b}{\beta_e \beta_b}, \qquad (3)$$

and I_e is the electron beam current.

Usually, as one can see from Fig. 1, the current density from the cathode is not radially uniform. If we further assume that the beam is axisymmetrical, then it is possible to create a normalized radial density profile $g(r)$ from the measured 2D profile (Fig. 2, red curve). Fig. 2 also shows the normalized electric field in the case of the measured radial profile. In simulations, we use a polynomial interpolation in order to obtain analytical expressions for the transverse kicks.

The lack of axial symmetry is of a particular importance when studying how the electron beam effects the circulating beam core. In this case, the electron beam can be represented by a δ-function cylinder in radius modulated by an angular charge distribution $f(\theta)$. This charge density can be decomposed into harmonics as follows:

$$\rho(r, \theta) = \frac{I_e}{\beta_e c} \frac{\delta(r - r_e)}{2\pi r_e} \sum_{m>0}^{\infty} \xi_m \cos(m\theta + \delta_m), \qquad (4)$$

where r_e is the electron beam radius, m is the harmonic number ($m = 1$ for dipole, $m = 2$ for quadrupole, etc.), ξ_m
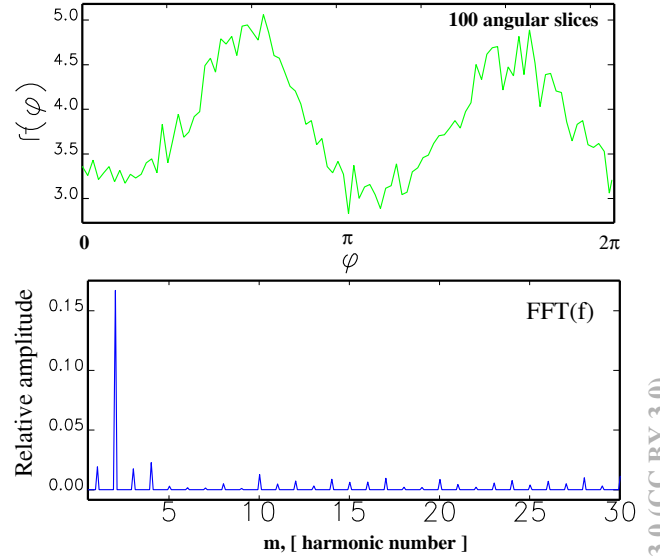
and δ_m are the amplitude (relative to the average) and phase of each harmonic. The parameters for each harmonic can be obtained from measurements (Figs. 1 and 3). Because we are interested in the effects on the beam core, we use the analytical expression for the transverse kicks due to each harmonic inside the cylinder:

$$\Delta p_x = -\Omega_e \Delta s \xi_m \frac{r^{m-1}}{r_e^m} \cos\left[(m-1)\theta + \delta_m\right] \qquad (5)$$

$$\Delta p_y = \Omega_e \Delta s \xi_m \frac{r^{m-1}}{r_e^m} \sin\left[(m-1)\theta + \delta_m\right]. \qquad (6)$$

RESULTS

Simulations were performed using the `Lifetrac` numerical tracking code [5] using the models described above, for different electron beam currents and pulsing patterns.

Figure 4 shows the particle loss rate normalized to the quadrupole harmonic for pulse regime '1/5', i.e. when the electron lens is turned on every sixth turn. The only significant effect appears for the quadrupole harmonic. This harmonic has the largest amplitude for all measured profiles. Most of the lost particles have initial amplitudes between 2σ and 3σ (σ being the standard deviation of the core population distribution). This effect is due to excitation of 12th order resonances, as it was verified with a frequency map analysis and by noting that calculated losses were reduced by changing the working point of the machine. For other pulse patterns no losses in the core were observed.

These results are in agreement with alignment simulations. The dipole harmonic gives no effect on the beam core as it equivalent to a small orbit bump. Transverse rotations also show no effect — simulations are not sensitive to the phases of the azimuthal harmonics. In principle, longitudi-
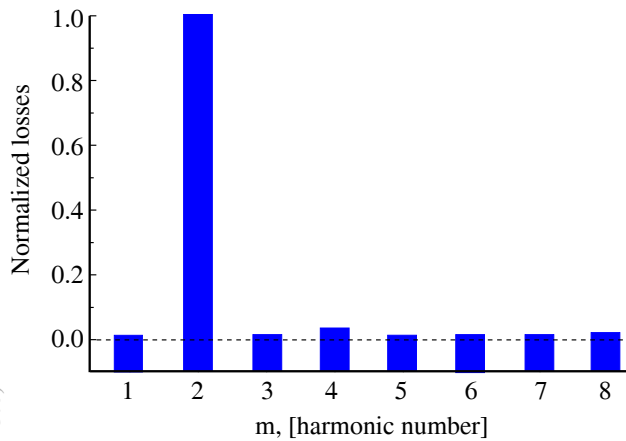
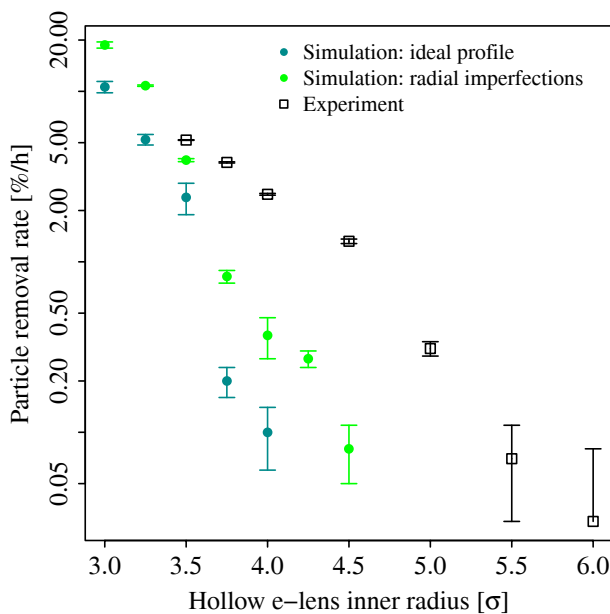Figure 4: Normalized particles loss rate for different azimuthal harmonics of the electron beam profile.

Figure 5: Comparison of halo loss rates for ideal model (cyan), nonuniform radial profile (green), and experiment (black).

nal rotations generate all possible harmonics, but only the quadrupole component applied with the 1/5 pulsing pattern showed significant effects.

Simulations of antiproton halo removal rates with different radial current profiles were compared with experiment [3]. The data was taken at different electron beam radii, and the electron lens was pulsed every turn in a region of the ring where the vertical amplitude function was much larger than the horizontal one. The vertical antiproton beam size was $\sigma_y = 0.06$ cm. A weighted Gaussian distribution containing 10,000 macroparticles was tracked for about 21 minutes of real time. The HEBC parameters were the following: length $L = 2$ m, electron beam current $I_e = 0.4$ A, and electron kinetic energy $K = 4.8$ keV. Re-
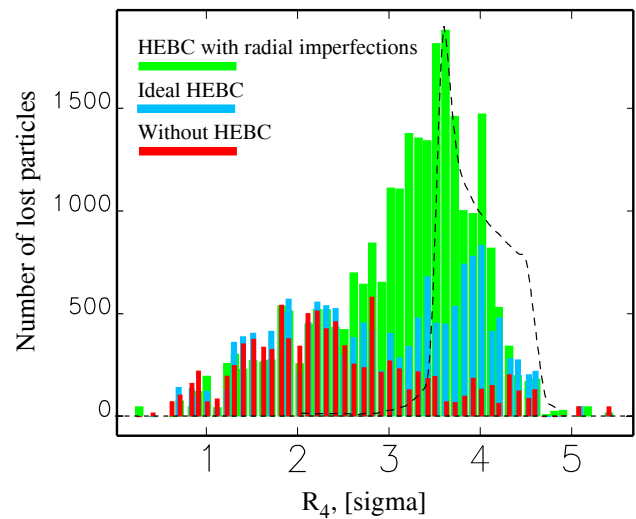

Figure 6: Distribution of lost particles vs. initial amplitude for electron beam matched to 3.5σ. The dashed line shows the radial electron beam profile.

sults are shown on Fig. 5. Numerical models give the correct order of magnitude for the halo removal rate ($\approx$%/h), but predicted loss rates are lower, with a stronger dependence on the hole radius. Figure 6 shows the number of lost particles as a function of their initial 4D amplitude, $R_4^2 = x^2 + p_x^2 + y^2 + p_y^2$. As expected, losses due to the HEBC appear in the regions of nonzero field.

These results suggest the following conclusions: (a) moderate electron beam currents enhance halo removal rates by a significant factor; (b) removal rates depend strongly on electron beam profile and on halo population, two factors that are not easily measurable directly; (c) if experimental data is not available, tracking codes can give rough but conservative estimates of the expected removal rates for other storage rings and colliders, such as the LHC.

REFERENCES

[1] V. Shiltsev, Proc. 3rd CARE-HHH-APD Workshop (LHC-LUMI-06), Valencia, Spain, p. 92, CERN-2007-002 (2007); V. Shiltsev, Proc. CARE-HHH-APD Workshop (BEAM07), Geneva, Switzerland, p. 46, CERN-2008-005 (2007); V. Shiltsev et al., Proc. 2008 Eur. Part. Accel. Conf. (EPAC08), Genoa, Italy, p. 292.

[2] G. Stancari et al., Proc. 2010 Int. Part. Accel. Conf. (IPAC10), Kyoto, Japan, p. 1698; Proc. 14th Adv. Accel. Concepts Workshop (AAC10), AIP Conf. Proc. **1299**, 638 (2010).

[3] G. Stancari et al., Phys. Rev. Lett. **107**, 084802 (2011); G. Stancari et al., Proc. 2nd Int. Part. Accel. Conf. (IPAC11), San Sebastián, Spain, p. 1939; G. Stancari et al., Proc. APS/DPB Meeting, Providence, Rhode Island, arXiv:1110.0144 [physics.acc-ph] (2011).

[4] E. Forest, Beam Dynamics: A New Attitude and Framework (Harwood Academic, Philadelphia, 1998).

[5] D. Shatilov et al., Proc. 2005 Part. Accel. Conf. (PAC05), Knoxville, p. 4138.